Electronics and Electrical Engineering

AIMS Electronics and Electrical Engineering, 9(3): 339–358.
DOI: 10.3934/electreng.2025016
Received: 09 April 2025
Revised: 28 May 2025
Accepted: 04 June 2025
Published: 12 June 2025

https://www.aimspress.com/journal/ElectrEng

Research article

Sensorless control of DC-DC buck converter using metaheuristic algorithm

Debarchita Mishra[1] and Sharmistha Mandal[2,*]

[1] Department of Electrical & Electronics Engineering, VELS Institute of Science, Technology and Advanced Studies, Chennai, India
[2] Department of Electrical Engineering, Aliah University, Kolkata, India

*** Correspondence:** Email: itssharmistha@gmail.com.

Abstract: The objective of this research work is to adjust the output voltage of a DC-DC buck converter under the influence of noise and parameter variations. For this purpose, a new Kalman filter-based fractional-order controller is proposed. The Kalman filter reduces the effects of sensor and process noise on the system output. To reduce the tuning intricacy of the fractional-order proportional-integral-derivative (FOPID) controller, circumvent the derivative term, and enhance system performance, a novel blended proportional-integral (BPI) controller is introduced. This controller combines integer-order and fractional-order proportional-integral controllers. The parameters of the proposed BPI controller are determined using four metaheuristic optimization techniques: firefly algorithm, artificial bee colony, particle swarm optimization, and Harris Hawks optimization. Among there, the potential of the firefly algorithm-based controller was superior to the other three controllers. The proposed controller is compared with the integer-order KF-based proportional-integral (PI) controller, proportional-integral-derivative (PID) controller, and KF-based fractional-order PI and PID controllers. The proposed controller presents better results regarding settling time and steady-state error. This controller also demonstrates better results under variations in input voltage and inductance of the buck converter. The results of the buck converter are compared with those from an artificial neural network (ANN)-based controller reported in previous literature. The proposed controller improves overshot by 96.42% and settling time by 40% when the inductance of the buck converter is reduced by 50% under a load change from 7.33 to 11 Ω.

Keywords: DC-DC buck converter; Kalman filter; proportional-integral controller; fractional-order controller; metaheuristic algorithm

1. Introduction

Power converters are increasingly employed in numerous applications, such as industrial electronics, portable devices, energy storage systems, and consumer electronics. In recent applications, such as artificial intelligence, networks related to the Internet of Things, and wireless sensors, power converters are critical components. Switch-mode DC-DC converters transfer the DC voltage from one level to another. High-level DC voltage is reduced to a low-level DC voltage by a DC-DC buck converter, which is widely used in modern-era applications such as photovoltaic systems, electric vehicles etc.

Regulating the output voltage of DC-DC converters in the presence of external noise and system parameter variations has proven to be challenging. Rigorous investigations are still ongoing in this subject, and different control algorithms have been proposed for controlling the output voltage of the converter. Chebyshev's neural network-based adaptive controller was designed to control the output voltage of a buck converter [1]. In another work, a new control algorithm was proposed to track the output voltage of a buck converter with overcurrent protection to hardware elements [2]. In Miao (2019) and Wang (2019), current-constrained controllers were proposed for the buck converter [3,4]. A linear matrix inequality-based H-infinity controller has been demonstrated to regulate the output voltage of buck and boost converters [5,6]. An artificial neural network (ANN)-based control algorithm was proposed for a DC-DC buck converter, and an optimal controller was designed using approximate dynamic programming [7]. Several observer-based control algorithms have been proposed, both for buck and boost converters [8–11]. A data-driven control algorithm was suggested for the interleaved DC-DC boost converter based on online integral reinforcement learning [12]. In 2022, the non-minimum-phase model of a boost converter was modified to a minimum-phase model for the purpose of controller design [13].

The proportional-integral-derivative (PID) controller and its modified versions are widely used in different applications. A sigmoid function-based data-driven proportional-integral (PI) controller was proposed to control the angular speed of a DC motor that is energized by a DC-DC converter [14]. Here, a sigmoid function represents the limits of the parameters of the PI controller. In [15], a neuroendocrine PID controller was designed for a multivariable crane system where the hormone discharge rate of neuroendocrine-PID can be regulated as per the error change. The output voltage of the DC-DC boost converter has been tracked using a brain emotional learning-based intelligent controller (BELBIC), where parameters are determined using the particle swarm optimization technique [16]. The performance of this controller outperformed the classical PID controller. Fractional-order proportional-integral (FOPI) and fractional-order proportional-integral-derivative (FOPID) controllers are very popular in industrial applications [17–19]. The FOPID controller is designed to stabilize the output power of the buck-boost converter for proton exchange membrane fuel cells [20]; an optimal FOPI controller was proposed for a solar photovoltaic system with a DC-DC boost converter [21]. The FOPID controller was also implemented in a real-time system, like a DC-DC boost converter and a magnetic levitation system [22,23]. A modified version of the FOPID controller, namely the tilt integral derivative (TID) and hybrid proportional integral derivative (PID) controllers, was proposed for load frequency control in multi-area interconnected power systems and second-order time delay systems, respectively [24,25].

Though different control techniques have been proposed for tracking the output voltage of the

DC-DC converter, the Kalman filter-based control algorithm has not been addressed before. The measurement of the output voltage of a DC-DC converter is essential for control purposes. However, measured outputs may be affected by the sensor noise. To deal with model uncertainty, noise must be considered. As a result, this research work designed a Kalman filter (KF) along with a controller to reduce the effects of sensor and process noises on the converter output. Modified versions of PID controllers have been employed for DC-DC converters, but some complications limit their widespread use. Instead, fractional-order PID controllers and variants have shown superior control abilities. Fractional-order proportional-integral (FOPID) controllers suffer from tuning complexity, and TID controllers are sensitive to parameter variations. To avoid these problems, a KF-based new controller, named blended proportional-integral (BPI) controller, is proposed to track the output voltage of the DC-DC buck converter. The BPI controller is a combination of FOPI and integer-order integral (I) controllers.

For parameter determination of the PID and FOPID controllers, optimization techniques are essential; for that purpose, metaheuristic algorithms like particle swarm optimization (PSO), artificial bee colony (ABC), genetic algorithm (GA), or firefly algorithm (FA) play a critical role [26]. The PID, FOPID, and FOPI parameters have been determined via the PSO technique [27], and a modified version of the sine-cosine algorithm was employed to estimate the PID controller parameters [28]. In [29], six parameters of a complex controller, which was a combination of the PID controller with an N-filter and a PD controller, were predicted using the golden eagle optimization technique. A new metaheuristic optimization technique, which is a combination of pattern search with opposition-based snake optimizer, was introduced and utilized to calculate the parameters of two cascaded first-order low-pass filters with the PID (PID-FF) controller [30]. Due to fast convergence rate, ease of implementation, and simplicity, the firefly algorithm (FA) was applied to estimate the parameters of the proposed BPI controller, which was introduced by Xin-She Yangin, 2008 [31]. This FA was then modified by different researchers and has been used in different applications for optimization purposes [32–35].

The contributions of the proposed work are presented below.

- A new Kalman filter-based controller is designed for the DC-DC buck converter. To control the output voltage of the converter, a blended proportional-integral (BPI) controller is proposed, which is the fractional order proportional-integral (FOPI) plus integer integral (I) controller.
- The parameters of the suggested controller are estimated using four metaheuristic optimization techniques: firefly algorithm (FA), artificial bee colony (ABC), particle swarm optimization (PSO), and Harris Hawks optimization (HHO). The FA-based controller outperforms the other three metaheuristic algorithms.
- The Kalman filter minimizes the effect of sensor and process noises on the output of the system, while the Kalman filter-based BPI controller tracks the output voltage of the converter with excellent transient response specifications in the presence of sensor and process noises. When the performance of the suggested BPI controller is compared with the PI, PID, FOPI, and FOPID controllers, BPI outperforms the others. The output of the closed-loop system is also compared with the artificial neural network-based controller presented by Dong et al., 2021 [7]; the proposed controller outperforms this controller.

2. Materials and methods

2.1. Dynamics of DC-DC buck converter

Figure 1 represents the circuit diagram of the buck converter. The circuit elements include the controlled switch MOSFET (S_{Bu}), diode (D_{Bu}), inductor (L_{Bu}) with internal resistance R_L, and capacitor (C_{Bu}) with internal resistance R_C, load resistance R, and DC input voltage V_{in}. The converter circuits with controlled switch (S_{Bu}) during on and off conditions are also shown. The parameter values for the buck converter circuit are given in Table 1 and are based on [7].

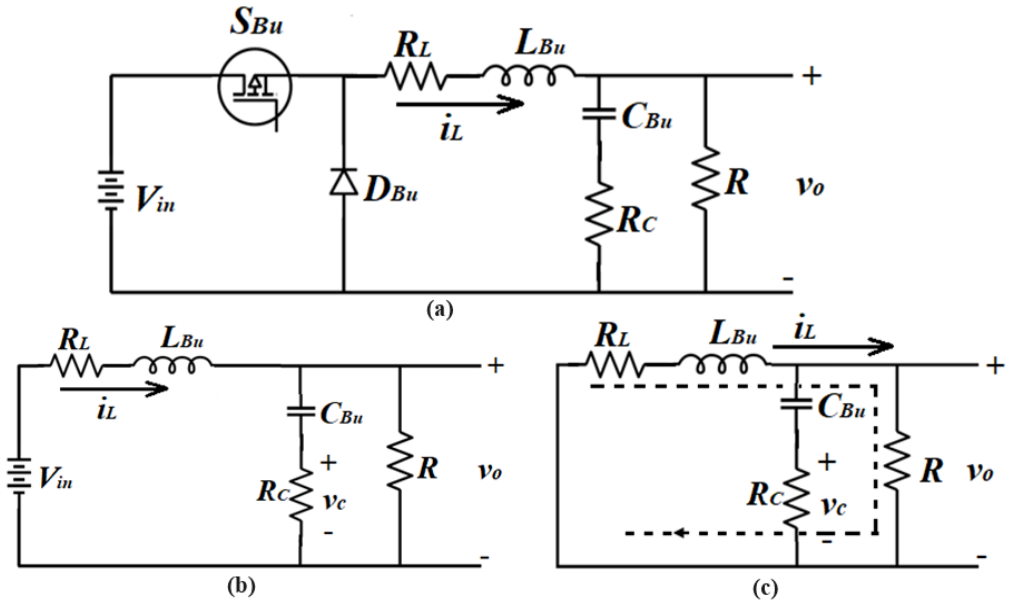

Figure 1. Buck converter circuit (a); on-mode circuit (b); off-mode circuit (c).

Table 1. Values of different parameters of the buck converter [7].

Parameter	Value
Input voltage, V_{in} (V)	42
Load resistance, R (Ω)	10
Internal resistance of inductor, R_L (Ω)	0.3
Internal resistance of capacitor, R_C (Ω)	0.02
Inductance, L_{Bu}(mH)	5.63
Capacitance, C_{Bu} (μF)	5

The voltage current of the converter during the **on** state is represented by the following equations:

$$V_{in} = R_L i_L + L_{Bu} \frac{d i_L}{dt} + v_0 \tag{1a}$$

$$C_{Bu} \cdot \frac{d v_c}{dt} = i_L - \frac{v_o}{R} \tag{1b}$$

$$v_o = R_C \left(i_L - \frac{v_o}{R} \right) + v_c \tag{1c}$$

where i_L and v_c are the inductor current and capacitor voltage, respectively, and v_o is the output voltage.

The equations below characterize the converter during the **off** state:

$$R_L i_L + L_{Bu} \frac{di_L}{dt} + v_0 = 0 \tag{2a}$$

$$C_{Bu} \cdot \frac{dv_c}{dt} = i_L - \frac{v_o}{R} \tag{2b}$$

$$v_o = R_C \left(i_L - \frac{v_o}{R} \right) + v_c \tag{2c}$$

Thus, the average model of the converter is given by the following equations:

$$DV_{in} = R_L i_L + L_{Bu} \frac{di_L}{dt} + v_0(t) \tag{3a}$$

$$C_{Bu} \cdot \frac{dv_c}{dt} = i_L - \frac{v_o}{R} \tag{3b}$$

$$v_o = R_C \left(i_L - \frac{v_o}{R} \right) + v_c \tag{3c}$$

Here, D represents the duty ratio (control input), which is provided by the pulse width modulator (PWM), and $D \in [0, 1]$.

The state-space model of the converter is illustrated below:

$$\begin{bmatrix} \frac{di_L}{dt} \\ \frac{dv_c}{dt} \end{bmatrix} = \begin{bmatrix} -\frac{1}{L_{Bu}} \left(\frac{RR_C}{R+R_c} + R_L \right) & -\frac{R}{L_{Bu}(R+R_c)} \\ \frac{1}{C_{Bu}} \left(1 + \frac{R_C}{R+R_c} \right) & -\frac{1}{(R+R_c).C_{Bu}} \end{bmatrix} \begin{bmatrix} i_L \\ v_c \end{bmatrix} + \begin{bmatrix} \frac{V_{in}}{L_{Bu}} \\ 0 \end{bmatrix} D \tag{4}$$

$$v_o = \begin{bmatrix} \frac{RR_c}{R+R_c} & \frac{R}{R+R_c} \end{bmatrix} \begin{bmatrix} i_L \\ v_c \end{bmatrix} \tag{5}$$

2.2. Kalman filter-based fractional-order controller

The Kalman filter-based controller is used to regulate the output voltage of the DC-DC buck converter. The parameters of the proposed BPI controller are determined by applying the metaheuristic firefly optimization technique. The block diagram of the buck converter with the Kalman filter-based controller is shown in Figure 2. The Kalman filter eliminates the effects of sensor and process noise on the output voltage, which is used for comparison with the reference voltage. The control input $u(t)$ is applied to the buck converter through the PWM.

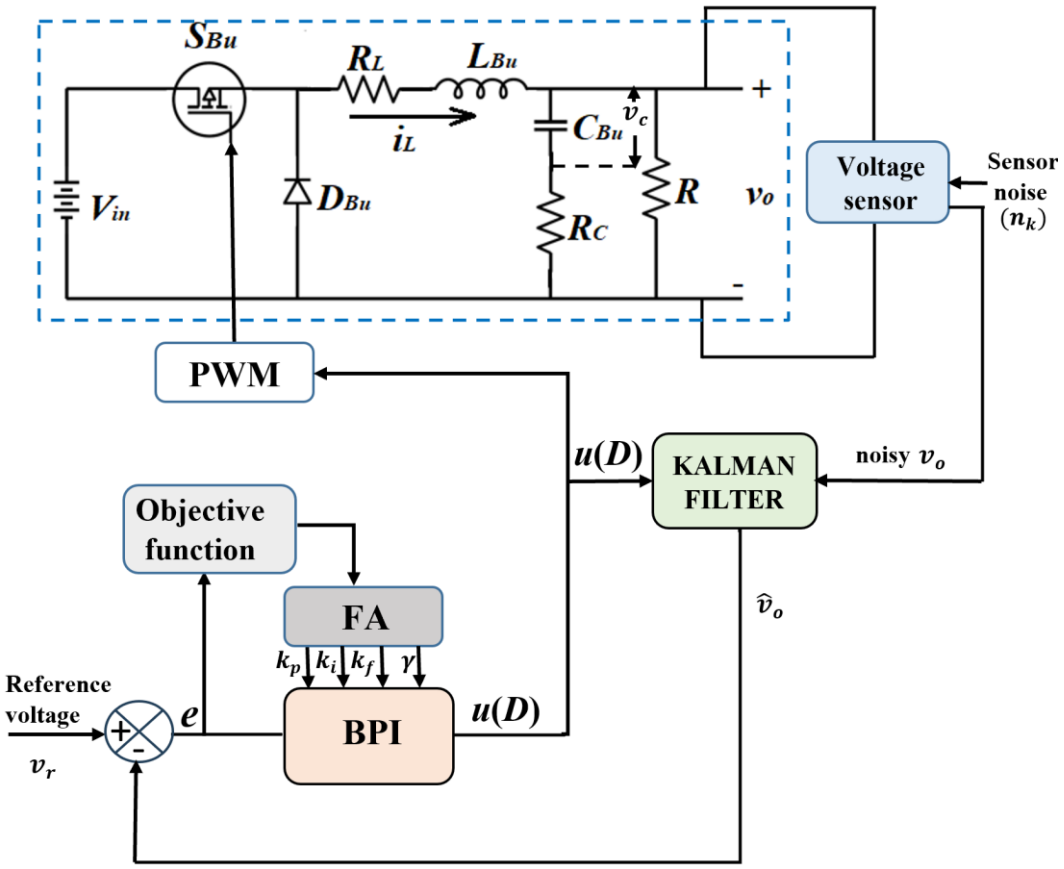

Figure 2. Buck converter with the Kalman filter-based BPI controller.

2.2.1. Kalman filter

The Kalman filter identifies the state variables of the system from the input and output data. This estimated output is used for control purposes. R. E. Kalman proposed the idea of the Kalman filter in 1960 [36]; since then, the Kalman filter and its modified versions have been used extensively in real-time systems for state estimation [37–41].

In discrete time domain, the state-space model of a linear time invariant is represented as

$$x_{k+1} = Ax_k + Bu_k + w_k \tag{6}$$

$$y_k = Cx_k + n_k = y_t + n_k \tag{7}$$

Here, k represents the time instant; $x \in \mathbb{R}^{n_x}$, $u \in \mathbb{R}^{n_u}$, and $y \in \mathbb{R}^{n_y}$ are the state, input, and measurement vectors, respectively; y_t is the output without sensor noise; w_k and n_k are the process and sensor noise, respectively.

It is assumed that process (w_k) and sensor (n_k) noises are Gaussian white noises with zero-mean and are mutually uncorrelated signals. The process and sensor noise covariance matrices are $E(w_k w_k^T) = Q$ and $E(n_k n_k^T) = R$, respectively. The algorithm of the Kalman filter is given in Table 2. The Kalman filter estimates the state variables of the system from the information of input and noisy output of the system. It estimates the state variables by minimizing the mean squared error $E[(x_k - \hat{x}_k)(x_k - \hat{x}_k)^T] = P_K$ where $\hat{x}_k$ is the prior estimated state vector and P_K is the error covariance matrix at k. These estimated states are free from sensor and process noise and are used for control

purposes. Accordingly, the Kalman filter minimizes the effects of noise on the output of the system. The algorithm of the Kalman filter is given in Table 2 [37].

Table 2. Kalman filter (KF) algorithm.

Step 1:	Mean value of states: $\hat{x}_0 = E(x_0) = x_{in}$
Initialization (k = 0)	Error covariance matrix: $P_0 = E[(x_0 - \hat{x}_0)(x_0 - \hat{x}_0)^T] = P_{in}$
Step 2:	Predicted state vector: $\hat{x}_{k+1\|k} = A\hat{x}_{k\|k} + Bu_k$
Prediction	A priori covariance matrix: $P_{k+1\|k} = AP_{k\|k}A^T + Q_w$
(time update)	
Step 3:	The updated state vector: $\hat{x}_{k+1\|k+1} = \hat{x}_{k+1\|k} + K_{k+1}[y_{k+1\|k} - C\hat{x}_{k+1\|k}]$
Correction	Posteriori covariance matrix: $P_{k+1\|k+1} = (I - K_{k+1}C)P_{k+1\|k}$
(measurement update)	The Kalman filter gain: $K_{k+1} = P_{k+1\|k}C^T(Q_v + CP_{k+1\|k}C^T)^{-1}$
	The algorithm returns to step 2.

It is challenging to select the process noise covariance matrix Q as it depends on model uncertainty. For this, Q is chosen by the trial-and-error method as $diag(0.00001, 0.00001)$. The sensor noise covariance (R) is chosen as 0.1, which depends on the accuracy of the voltage sensor. The Kalman filter is implemented using MATLAB software, and the state estimation error covariance matrix becomes $\begin{bmatrix} 2.728 \times 10^{-7} & 2.725 \times\times 10^{-8} \\ 2.725 \times 10^{-8} & 2.975 \times 10^{-9} \end{bmatrix}$. The resulting Kalman filter estimates the state variables i_L and v_c accurately, and accuracy is computed in terms of root mean square error (RMSE) given by $RMSE = \left(\frac{\sum_{k=1}^{T_s}(x_1 - \hat{x}_1)^2}{T_s}\right)^{1/2}$, where x_1 and $\hat{x}_1$ are the actual and estimated state variables, respectively. The RMSE values of state variables i_L and v_c are 0.1261 and 0.2167, respectively. The covariance of the measured error (error between y_t and measured output, y) and the estimated error (error between y_t and estimated output, $\hat{y}$) are 0.0994 and 0.0465, respectively. From these covariances, it can be concluded that KF minimizes the effect of noise on the output of the system.

2.2.2. Blended proportional-integral (BPI) controller

Linear controllers, as the integer and fractional-order proportional-integral (PI) and proportional-integral-derivative (PID) controllers, are used extensively for the fulfillment of the transient as well as steady-state response specifications of the system. The transfer function of PID and fractional-order PID (FOPID) controllers is as follows [17,18].

$$G_{PID}(s) = k_p + \frac{k_i}{s} + k_d s; \quad G_{FOPID}(s) = k_p + \frac{k_i}{s^\lambda} + k_d s^\mu$$

where k_p, k_d, and k_i are the gain of the proportional, derivative, and integral controllers, respectively; λ and μ are real fractional numbers ($0 \leq (\lambda, \mu) \leq 1$).

The FOPID has more control on the system than PID, since the former has five control parameters, as opposed to the three from PID. Still, the issue lies in optimizing these five parameters in FOPID instead of the three in PID.

For this study, a new fractional-order controller is proposed, which is a combination of integer and fractional-order PI controllers and is named the blended proportional-integral (BPI) controller.

The structure of the controller is shown in Figure 3, and the transfer function of the controller is given by

$$G_{BPI}(s) = k_p + \frac{k_i}{s} + \frac{k_f}{s^\lambda}$$

where k_p is the gain of the proportional controller, k_i is the gain of the integer-order integral controller, k_f is the gain of the fractional-order integral controller, and the exponent λ is a real number ($0 \leq \lambda \leq 1$).

The number of parameters that need to be optimized for the BPI controller is four, which is less than the FOPID (five parameters). The merit of the BPI controller over other fractional-order controllers like FOPID and TID is that it has no derivative term. Actually, the derivative term is required to damp out oscillations, but it can strengthen noise if parameter estimations are incorrect. The results section proves that BPI presents robust performance when facing parameter variations and noise.

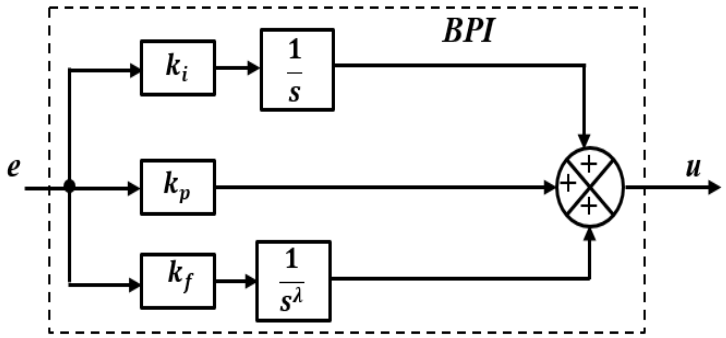

Figure 3. Structure of BPI controller.

2.2.3. Firefly algorithm for the design of BPI controller

The firefly algorithm (FA) is an extremely popular metaheuristic optimization technique that takes inspiration from nature and is extensively used for solving engineering problems. In this algorithm, the objective function changes proportionally with the brightness of the firefly; this means that when brightness is reduced, the firefly will travel or search for a brighter firefly. If there is no brighter firefly, then the firefly will move aimlessly.

Consider there are *n* fireflies where $f(d)$ represents the fitness function or objective function. The brightness of a firefly (I_i) determines the current position d_i. The distance between two fireflies is given [31,32] by

$$r_{ij} = \left\| d_i - d_j \right\| = \sum_{k=1}^{k=n} (d_{ik} - d_{jk})^2 \tag{8}$$

where d_i and d_j represent the position of i^{th} and j^{th} fireflies, respectively.

The relationship between the attractiveness function β and distance r is $\beta = \beta_0 e^{-\gamma r^2}$, where β_0 signifies the attractiveness at $r = 0$ and the light absorption coefficient is denoted by γ.

Suppose that in a *t*-th iteration, the firefly i at position d_i is moved to a brighter firefly j. Now, the new position of firefly i in $(t+1)$-th iteration is expressed by the following equation [33,34]:

$$d_i(t+1) = d_i(t) + \beta_0 e^{-\gamma r_{ij}^2} \left(d_j(t) - d_i(t) \right) + \alpha \epsilon_i \tag{9}$$

where $d_i(t)$ represents the old position of firefly i; ϵ_i is a random number that can be determined from Gaussian, uniform, or any other distribution; α is called the randomization parameter $(0 \leq \alpha \leq 1)$.

The pseudocode of FA is illustrated in Table 3. Optimization problems like extremely nonlinear and multi-modal can be handled efficiently using FA; its speed of convergence is also extraordinary.

Table 3. Algorithm of the firefly optimization technique.

Pseudocode of firefly algorithm (FA)
• **Input**: Number of fireflies (n), no. of maximum iterations (*MaxIter*), attractiveness factor (β_0), randomization parameter (α), light absorption coefficient (γ).
• **Output**: Best result originated by the FA.
1. **Initialization of** n, *MaxIter*,β_0,α, γ.
2. Determine initial population of fireflies d_i, where $i = 1,2, \dots, n$.
3. Define objective function $f(d)$ where $d = [d_1, \dots, d_n]^T$.
4. Calculate light intensity I_i for firefly at d_i using $f(d_i)$ for all fireflies
Main Loop
5. **While** $(t < MaxIter)$
For $i = 1$ to n
For $j = 1$ to n
if $(I_j > I_i)$
Travel firefly i towards firefly j according to equation (9)
end if
Evaluate new $f(d_i)$ and light intensity I_i
end for j
end for i
Rank the fireflies and determine the best global solution
end while

For the optimization, the fitness function or cost function is considered as integral time absolute error (ITAE), which computes the integral of the product of the absolute value of difference between reference input and actual output and time. The ITAE is given by

$$f\left(k_p, k_i, k_{f,} \lambda\right) = ITAE = \int_0^t t|v_r - \hat{v}_o|dt$$

where v_r and $\hat{v}_o$ are the reference voltage and estimated output voltage by Kalman filter respectively.

One of the key objectives of this research work is to minimize the time response specifications, like maximum peak overshoot, settling time, and steady-state error. The cost function ITAE fulfils these requirements better than other cost functions, like integral square error (ISE) and integral absolute error (IAE). The design procedure of the BPI controller using the FA algorithm is presented in Figure 4.

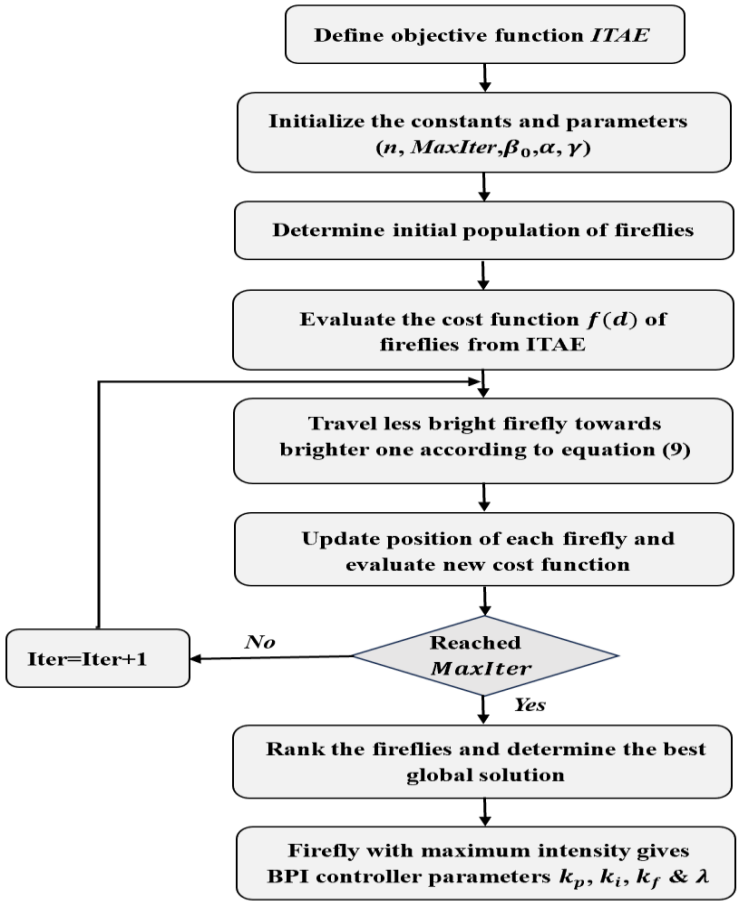

Figure 4. Design procedure of the BPI controller using the FA algorithm.

3. Results

The values of different parameters used for the buck converter are presented in Section 2.1 [7]. The transfer function of the considered DC-DC buck converter is $G(s) = \frac{(148.9s+1.489\times10^9)}{(S^2+2.002\times10^4 s+3.652\times10^7)}$.

For the BPI controller, four parameters, k_p, k_i, k_f, and λ need to be optimized using the optimization technique FA. The lower limit (LL) and upper limit (UL) of these four parameters are chosen from experience as follows:

$k_p = [0.001(LL) \quad 0.09(UL)]$; $k_i = [0.001(LL) \quad 10(UL)]$; $k_f = [0.001(LL) \quad 6(UL)]$;
$\lambda = [0.001(LL) \quad 0.999(UL)]$.

Applying FA, the gains of the controller BPI are optimized considering the cost function ITAE, ISE, and IAE. The best cost function versus the number of iteration curves is shown in Figure 5a for 25 iterations.

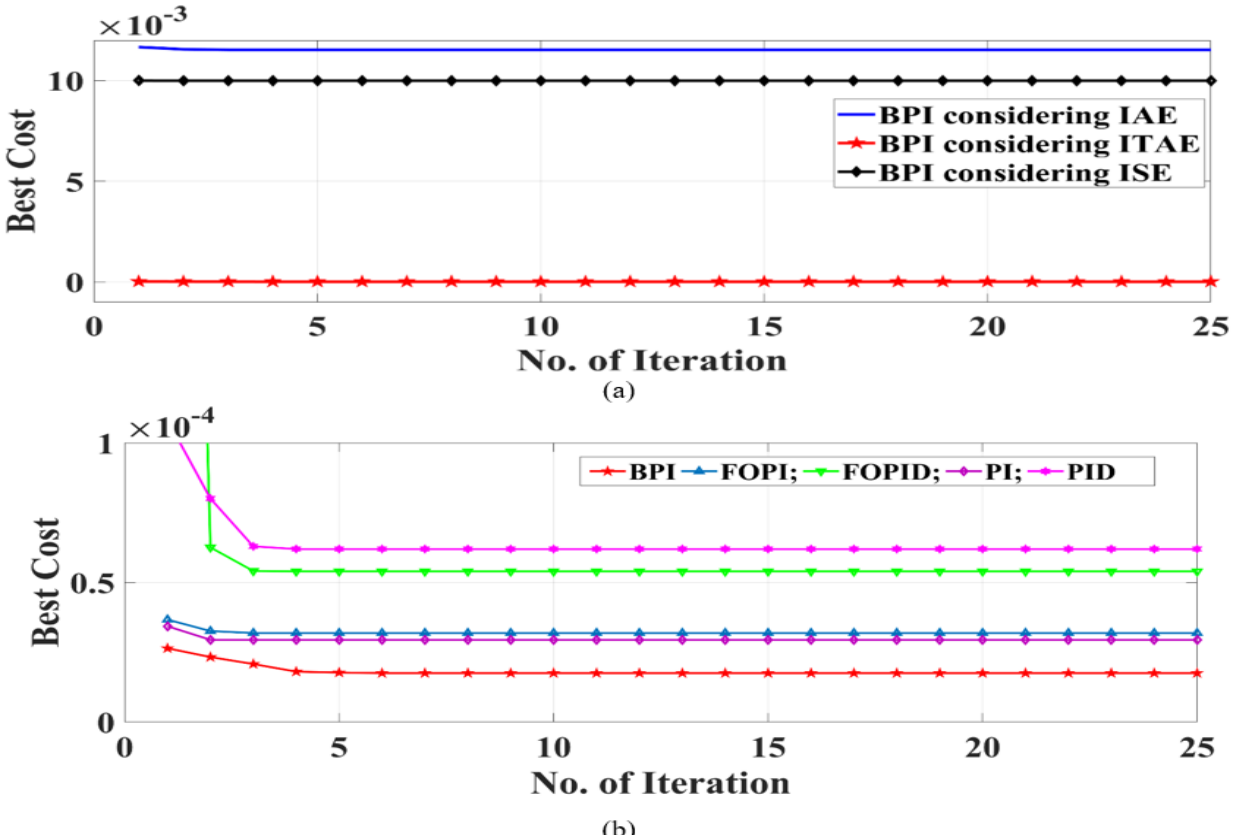

Figure 5. Fitness function vs. number of iteration curve (a) for different cost functions and (b) for different controllers.

Table 4. Parameters of different controllers obtained using different metaheuristic algorithms.

Optimization technique	Control algorithm	Value of the parameters					
		k_p	k_i	k_d	k_f	λ	μ
	PI	0.001	9.8729	-	-	-	-
	PID	0.0998	10	0.0362	-	-	-
	FOPI	0.0012	9.9803	-	-	0.999	-
FA	FOPID	0.001	9.9317	0.0157		0.999	0.001
	BPI	0.0017	9.99	-	5.9858	0.999	-
ABC	BPI	0.0112	10	-	6	0.999	-
PSO	BPI	0.001	10	-	6	0.999	-
HHO	BPI	0.09	10	-	6	0.999	-

In this case, PI, PID, FOPI, and FOPID controllers are also designed for the buck converter using FA to compare the potential of BPI. Table 4 represents the values of the parameters of the different controllers. The objective function ITAE vs. the number of iterations (25 iterations) of different controllers is shown in Figure 5b; it shows that, among all controllers, BPI provides the minimum value of ITAE. The fractional-order controller blocks are obtained using the FOMCON toolbox. Figure 6 represents the closed-loop output voltage and inductor current responses of the buck converter with Kalman filter-based controllers for an 18 V reference voltage. Performance measures of different controllers are given in Table 5.

Table 5. Performance measures of different controllers using different metaheuristic algorithms.

	Time response specifications	Settling-time (s)	Maximum overshoot	Under shoot	Integral time absolute error (ITAE)	Integral square error (ISE)	Integral absolute error (IAE)
FA-based	PI	0.0095	0	0	9.108×10^{-5}	0.4736	0.04471
	PID	0.001	4.54%	0	0.0007329	0.05703	0.03065
	FOPI	0.0095	0	0	9.125×10^{-5}	0.4636	0.04412
	FOPID	0.02	0	0	0.0001613	0.3343	0.04433
	BPI	0.0055	0.06%	0	3.101×10^{-5}	0.3177	0.02766
ABC-based	BPI	0.01	0%	0	4.672×10^{-5}	0.2337	0.02756
PSO-based	BPI	0.0051	0.236%	0	3.044×10^{-5}	0.3261	0.02774
HHO-based	BPI	0.028	0%	0	0.0001776	0.08423	0.02754

To test the performance of the Kalman filter, outputs are collected for a reference voltage of 18V with a sensor noise power of 0.1 and process noise power of 0.000001. The output voltage and inductor current of the buck converter with a KF-based BPI controller and without KF (only with BPI controller) are shown in Figure 7.

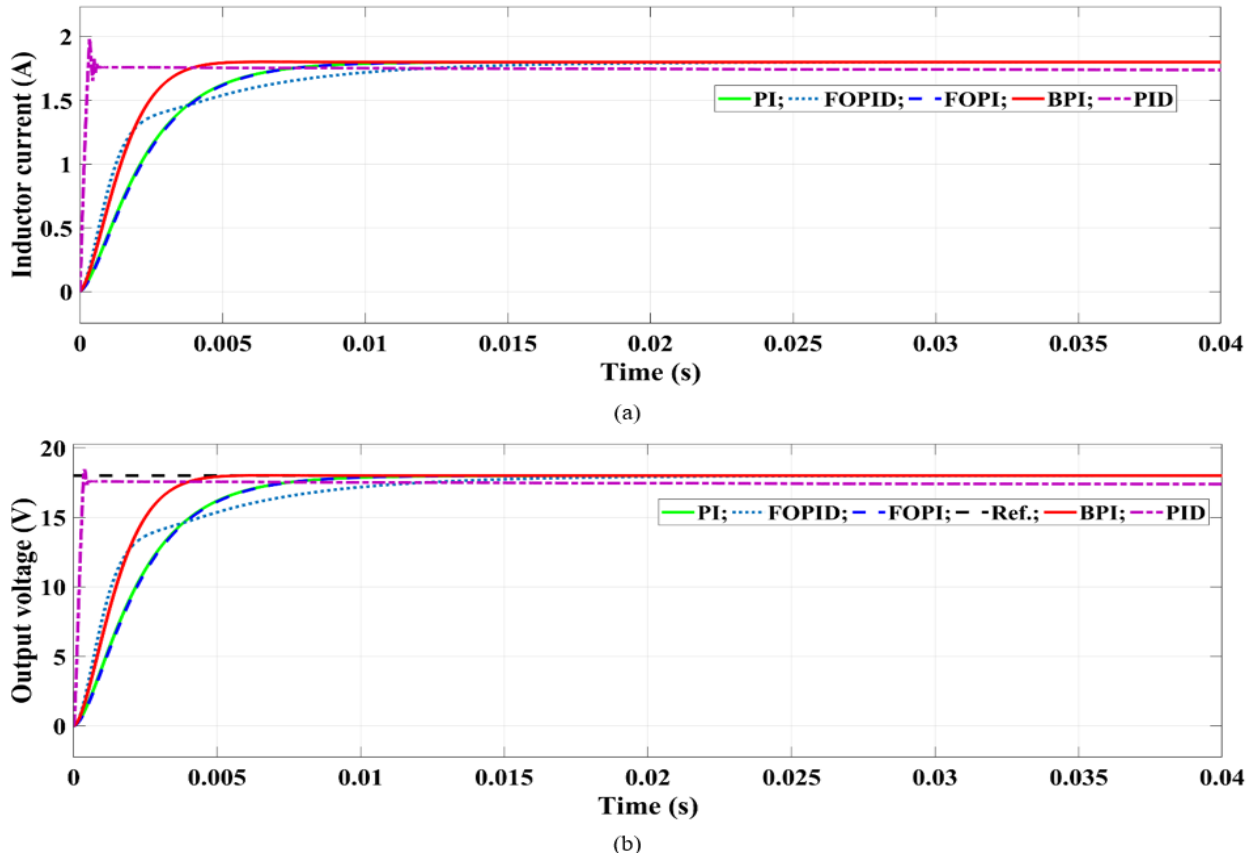

Figure 6. Output voltage (a) and inductor current (b) of the buck converter with different controllers.

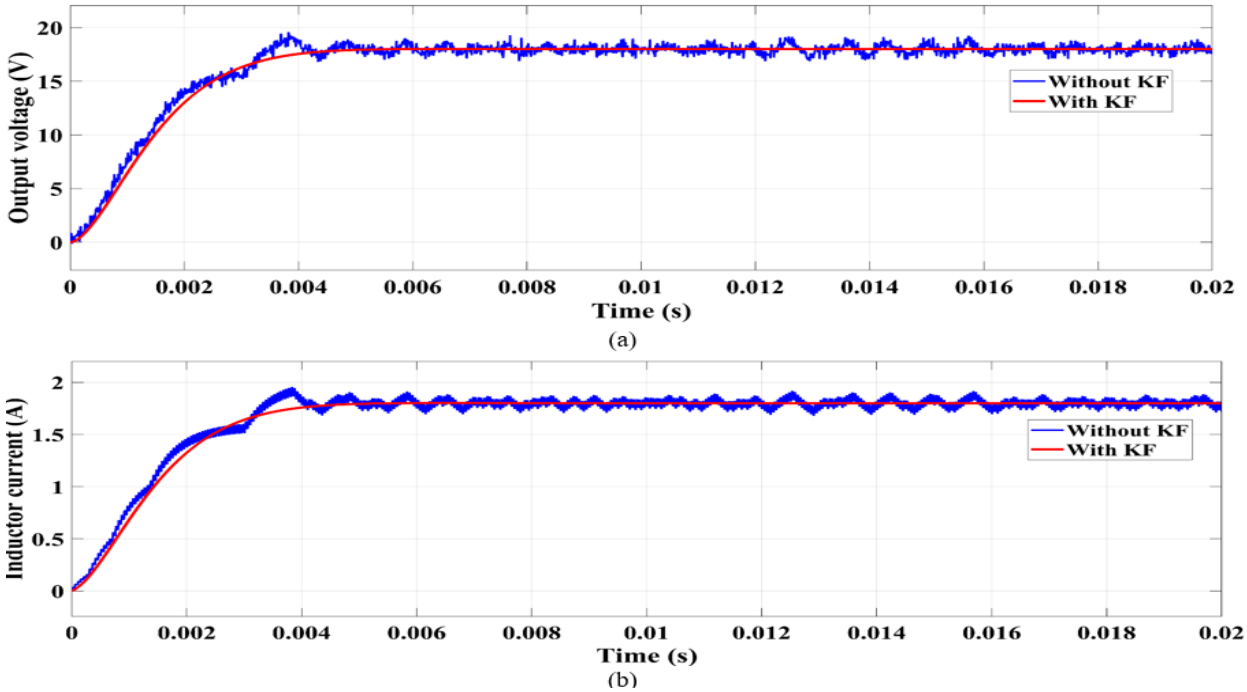

Figure 7. Output voltage of the closed-loop system with and without the Kalman filter.

3.1. Comparison with other metaheuristic algorithms

Besides the firefly algorithm (FA), three other metaheuristic algorithms [artificial bee colony (ABC), particle swarm optimization (PSO), and Harris Hawks optimization (HHO)] were used to estimate parameters (k_p, k_i, k_f, and λ) of the BPI controller. The algorithms of these optimization techniques are given in the literature [42]. The estimated parameters of the BPI controller using these four optimization techniques are presented in Table 4. Performance measures of different optimization techniques for the KF-based BPI controllers are given in Table 5 and shown in Figure 8.

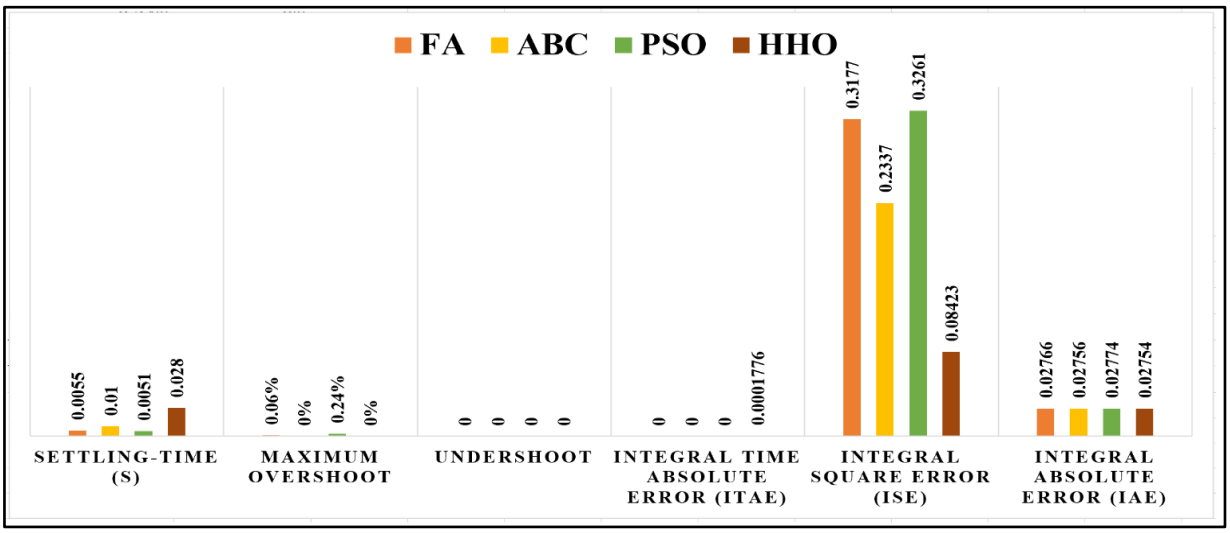

Figure 8. Performance measures of different algorithm-based BPI controllers with KF.

The statistical analysis of the fitness function (ITAE) with different optimization algorithms is presented in Table 6. As the metaheuristic algorithms FA, PSO, ABC, and HHO are stochastic in nature, the best value, standard deviation, and mean value of ITAE are calculated for 15 individual trials. The p-value of Wilcoxon's rank-sum test is also calculated and provided in Table 6. Wilcoxon's test, a nonparametric test, is used to compare two paired groups. A p-value lower than 0.05 means there is no variance between the two compared groups.

Table 6. Statistical analysis of fitness function (ITAE) for different optimization algorithms.

Algorithm	Best	Standard deviation	Mean	Wilcoxon's rank-sum test p-value FA (BPI) vs
FA (BPI)	$\mathbf{1.75\times10^{-5}}$	$\mathbf{1.81548\times10^{-6}}$	$\mathbf{1.88\times10^{-5}}$	
ABC (BPI)	1.77×10^{-5}	6.36946×10^{-6}	2.54×10^{-5}	6.0111×10^{-4}
HHO (BPI)	1.78×10^{-5}	4.55625×10^{-6}	2.34×10^{-5}	0.0012
PSO (BPI)	1.77×10^{-5}	5.10655×10^{-6}	2.30×10^{-5}	0.0047

3.2. Comparison with other control techniques

For comparison with the proposed KF-based BPI controller, an artificial neural network (ANN) -based controller, suggested by Dong (2021), was considered. The same system is considered, and simulation results are compared in both cases. The KF-based BPI controller is tested with the same load and parameter variations as mentioned in [7]. Responses under various conditions are illustrated in Figure 9, and performance measures are given in Table 7.

Table 7. Performance comparison with the ANN-based controller.

Changed condition	% Overshoot		Settling time (s)	
	ANN controller	**Proposed controller**	**ANN controller**	**Proposed controller**
Load resistance R changes from 7.33 to 11 Ω	38.89%	1.39%	0.002	0.002
Reference voltage v_r varies from 18 to 24 V	0%	0%	0.007	0.005
Input voltage V_{in} is changed from 42 to 47 V	4.44%	17.2%	0.006	0.0035
Inductance L_{Bu} decreases by 50% and load resistance R changes from 7.33 to 11 Ω	38.89%	1.39%	0.005	0.003
Inductance L_{Bu} decreases by 85% and load resistance R changes from 7.33 to 11 Ω	44.44%	1.66%	0.0017	0.0018

Table 6 shows that the proposed BPI controller performs better than the ANN-based controller in terms of overshoot and settling time. Some ringing (oscillations) can be seen in both voltage and current waveforms for the ANN-based controller, which is not present at all in the proposed BPI controller.

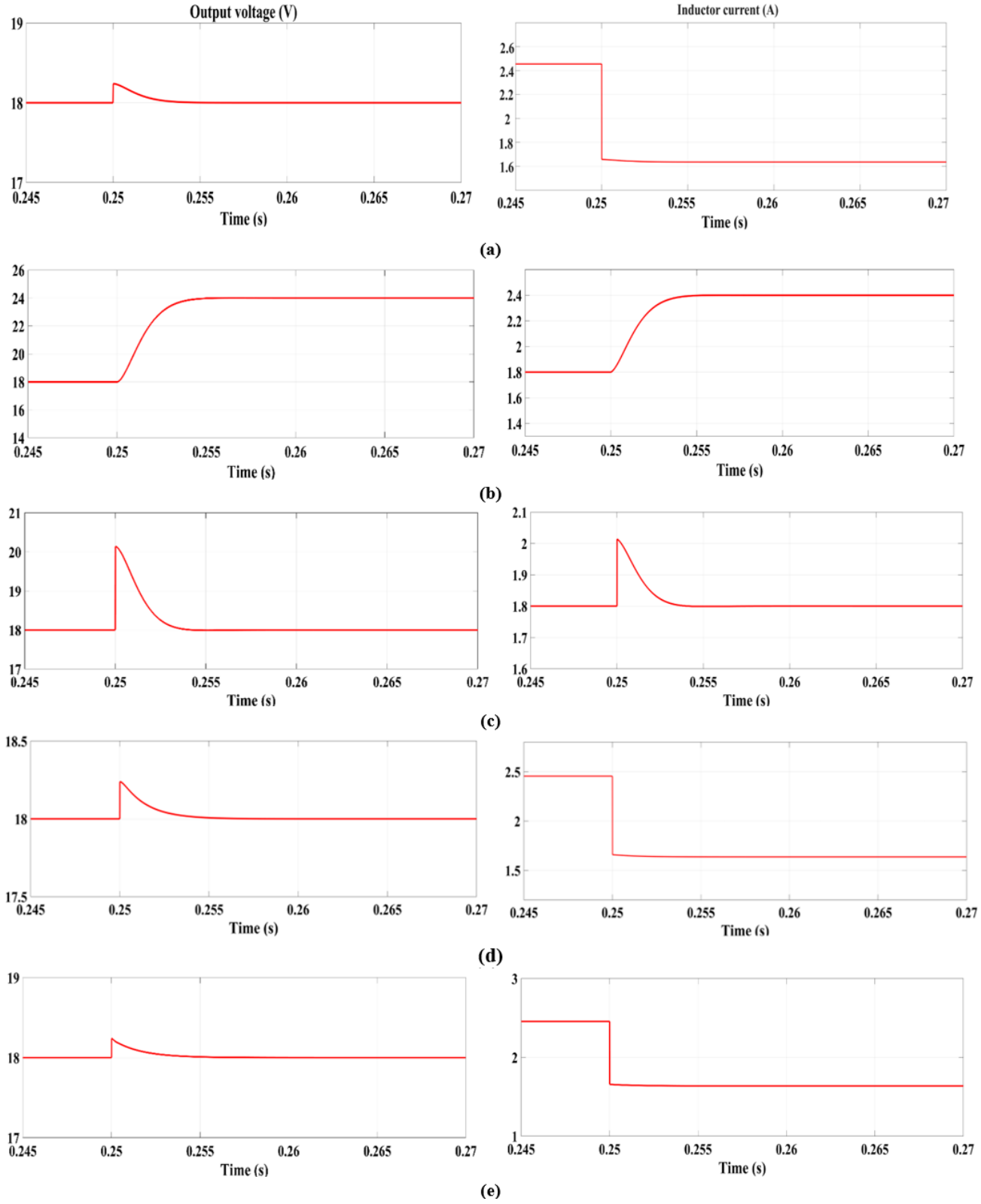

Figure 9. Output voltage and inductor current responses when (a) load changes from 7.33 to 11 Ω; (b) reference voltage varies from 18 to 24 V; (c) input voltage V_{in} changes from 42 to 47 V; (d) L_{Bu} decreases by 50% with the same load change as in (a); (e) L_{Bu} decreases by 85% with the same load change as in (a).

4. Discussion

The best cost function values for IAE, ISE, and ITAE were 0.011533, 0.010004, and 1.75×10^{-5}, respectively. From the convergence curve (Figure 5a) and these cost values, it is evident that ITAE provides better results than the other cost functions.

From Table 5, it is clear that the proposed BPI controller demonstrates better performance in terms of settling time, ITAE, and IAE than the other designed controllers. Figure 6 shows that the output voltage with the KF-based BPI controller accurately tracks the reference voltage of 18 V, with a negligible amount of overshoot in both the output voltage and inductor current waveforms. Hence, the BPI controller is considered for the regulation of the output voltage of the buck converter.

From Figure 7, it is clear that the converter outputs with the KF-based BPI controller are not influenced by the sensor and process noise; Additionally, the controller provides overcurrent protection to the hardware components of the buck converter. This indicates that the KF eliminates the influence of sensor and process noise on the system output.

Table 5 shows that the ABC and HHO-based BPI controllers are capable of producing zero overshoot, but the settling time are higher than with the FA and PSO-based controllers. Also, the maximum peak overshoot of the PSO-based controller is greater than that of the FA-based controller. By comparing these performance measures, it is clear that the FA-based BPI controller outperforms the other three metaheuristic algorithm-based controllers. From Table 6, it is clear that the FA-based BPI controller provides the lowest best value, standard deviation, and mean value compared to the other techniques.

Figure 9 shows the responses of the KF-based BPI controller under various parameter variations. A performance comparison between the proposed controller and the ANN-based controller [7] is presented in Table 7. The BPI controller improves maximum overshoot by 96.42% compared to the ANN controller under load resistance variations.

5. Conclusions

This study describes the design of a new Kalman filter-based blended proportional-integral (BPI) controller and demonstrates the regulation of the output voltage of a DC-DC buck converter. The responses with and without the Kalman filter reveal that it eliminates the effect of sensor and process noises on the output voltage. The proposed fractional-order KF-based BPI controller gives better time response with respect to settling time, maximum overshoot, and ITAE than other KF-based controllers like PI, PID, FOPI, and FOPID. Statistical analysis shows that the performance of the proposed FA-based controller is superior to that of other metaheuristic algorithms. A comparative study also shows that the KF-based BPI controller outperforms other control techniques like ANN: the peak value of the voltage and transient time is much lower for the BPI controller than the ANN controller under different load conditions and parameter variations. The BPI controller decreases the maximum overshoot by 96.26% when the inductance of the buck converter is reduced by 85% under a load change from 7.33 Ω to 11 Ω. Hence, the proposed controller is capable to provide excellent transient responses and robust performance. In the future, the proposed control algorithm may be experimentally validated with a real-time system.

Author contributions

Debarchita Mishra: Conceptualization, simulation, writing – original draft; Sharmistha Mandal:

Analysis, drafting and editing of the manuscript.

Use of Generative-AI tools declaration

The authors declare they have not used Artificial Intelligence (AI) tools in the creation of this article.

Conflict of interest

On behalf of all authors, the corresponding author declare that they have no known competing financial interests or personal relationships that could have appeared to influence the work reported in this paper.

References

1. Nizami TK, Mahanta C (2016) An intelligent adaptive control of DC–DC buck converters. *J Franklin Ins* 353: 2588–613. https://doi.org/10.1016/j.jfranklin.2016.04.008
2. Guo T, Wang Z, Wang X, Li S, Li Q (2017) A simple control approach for buck converters with current-constrained technique. *IEEE T Contr Syst Tech* 27: 418–425. https://doi.org/10.1109/TCST.2017.2758347
3. Miao Q, Sun Z, Zhang X (2019) Non smooth current-constrained control for a DC–DC synchronous buck converter with disturbances via finite-time-convergent extended state observers. *Electronics* 9: 16. https://doi.org/10.3390/electronics9010016
4. Wang Z, Guo T, Wang X, Li S (2019) GPI observer-based composite current-constrained control approach for DC–DC buck converters. *The Journal of Engineering* 2019: 581–586. https://doi.org/10.1049/joe.2018.9386
5. Mandal S, Mishra D (2018) Robust control of buck converter using H-infinity control algorithm. *IEEE Applied Signal Processing Conference (ASPCON)*, Kolkata, 163–167. https://doi.org/10.1109/ASPCON.2018.8748623
6. Mishra D, Mandal S (2020) Voltage Regulation of DC-DC Boost Converter using H-infinity Controller. *2020 International Symposium on Devices, Circuits and Systems (ISDCS)*, 1–5. https://doi.org/10.1109/ISDCS49393.2020.9263019
7. Dong W, Li S, Fu X, Li Z (2021) Fairbank, M., Gao, Y.: Control of a buck DC/DC converter using approximate dynamic programming and artificial neural networks. *IEEE Transactions on Circuits and Systems I: Regular Papers* 68: 1760–1768. https://doi.org/10.1109/TCSI.2021.3053468
8. He W, Namazi MM, Koofigar HR, Amirian MA, Blaabjerg F (2021) Stabilization of DC–DC buck converter with unknown constant power load via passivity-based control plus proportion-integration. *IET Power Electron* 14: 2597–609. https://doi.org/10.1049/pel2.12205
9. He W, Shang Y, Namazi MM, Ortega R (2022) Adaptive sensorless control for buck converter with constant power load. *Control Eng Pract* 126: 105237. https://doi.org/10.1016/j.conengprac.2022.105237
10. Kim SK, Ahn CK (2018) Self-Tuning Proportional-Type Performance Recovery Property Output Voltage-Tracking Algorithm for DC–DC Boost Converter. *IEEE T Ind Electr* 66: 3167–3175. https://doi.org/10.1109/TIE.2018.2849982

11. Kim SK (2018) Output voltage-tracking controller with performance recovery property for DC/DC boost converters. *IEEE T Contr Syst Tech* 27: 1301–1307. https://doi.org/10.1109/TCST.2018.2806366
12. Qie T, Zhang X, Xiang CQ, Yu Y, Iu HHC, Fernando T (2022) A new robust integral reinforcement learning based control algorithm for interleaved DC/DC boost converter. *IEEE T Ind Electr* 70: 3729–3739. https://doi.org/10.1109/TIE.2022.3179558
13. Errouissi R, Shareef H, Viswambharan A, Wahyudie A (2022) Disturbance observer-based feedback linearization control for stabilization and accurate voltage tracking of a DC-DC boost converter. *IEEE T Ind Appl* 58: 6687–6700. https://doi.org/10.1109/TIA.2022.3183040
14. Ahmad MA, Ismail RMTR (2017) A data-driven sigmoid-based PI controller for buck-converter powered DC motor. *2017 IEEE Symposium on Computer Applications & Industrial Electronics* (*ISCAIE*), 81–86. https://doi.org/10.1109/ISCAIE.2017.8074954
15. Ghazali MR, Ahmad MA, Raja Ismail RMT, Tokhi MO (2019) An improved neuroendocrine–proportional–integral–derivative controller with sigmoid-based secretion rate for nonlinear multi-input–multi-output crane systems. *J Low Freq Noise Vib Act Control* 39: 1172–1186. https://doi.org/10.1177/1461348419867524
16. Azari AN, Sarfi G (2018) Robust Intelligent Controller for Voltage Stabilization of dc-dc Boost Converters. *International Research Journal of Engineering and Technology* (*IRJET*) 5: 377–385.
17. Yeroglu C, Tan N (2011) Note on fractional -order proportional-integral-differential controller design. *IET Control Theory Application* 5: 1978–1989. https://doi.org/10.1049/iet-cta.2010.0746
18. Tepljakov A, Alagoz BB, Yeroglu C, Gonzalez E, HosseinNia SH, Petlenkov E (2018) FOPID Controllers and Their Industrial Applications: A Survey of Recent. *IFAC-Papers on Line* 51: 25–30. https://doi.org/10.1016/j.ifacol.2018.06.014
19. Moreira WEM, Garcia C (2021) Performance comparison between IOPID and FOPID controllers in an industrial flow pilot plant. *IFAC Papers on Line* 54: 232–237. https://doi.org/10.1016/j.ifacol.2021.10.039
20. Qi Z, Tang J, Pei J, Shan L (2020) Fractional Controller Design of a DC-DC Converter for PEMFC. *IEEE Access* 8: 120134–120144. https://doi.org/10.1109/ACCESS.2020.3005439
21. Mohamed AT, Mahmoud MF, Swief RA, Said LA, Radwan AG (2021) Optimal fractional-order PI with DC-DC converter and PV system. *Ain Shams Eng J* 12: 1895–1906. https://doi.org/10.1016/j.asej.2021.01.005
22. Seo SW, Choi HH (2019) Digital Implementation of Fractional Order PID-Type Controller for Boost DC–DC Converter. *IEEE Access* 7: 142652–142662. https://doi.org/10.1109/ACCESS.2019.2945065
23. Acharya DS, Mishra SK, Swain SK, Ghosh S (2022) Real-Time Implementation of Fractional-Order PID Controller for Magnetic Levitation Plant with Time Delay. *IEEE T Instrum Meas* 71: 1–11. https://doi.org/10.1109/TIM.2022.3218566
24. Sahu RK, Panda S, Biswal A, Chandra Sekhar GT (2016) Design and analysis of tilt integral derivative controller with filter for load frequency control of multi-area interconnected power systems. *ISA Transactions* 61: 251–264. https://doi.org/10.1016/j.isatra.2015.12.001
25. Hanif O, Shree RS (2019) Design and Analysis of Proportional Integral Derivative Controller and its hybrids. *2019 IEEE 5th International Conference for Convergence in Technology (I2CT)*, 1–6. https://doi.org/10.1109/I2CT45611.2019.9033684

26. Joseph SB, Dada EG, Abidemi A, Oyewola DO, Khammas BM (2022) Metaheuristic algorithms for PID controller parameters tuning: review, approaches and open problems, *Heliyon* 8. https://doi.org/10.1016/j.heliyon.2022.e09399
27. Mandal S, Afza A (2023) Liquid Level Control of Coupled Tank System Using FOPID Controller. In: Rani, A., Kumar, B., Shrivastava, V., Bansal, R.C. (eds) Signals, Machines and Automation. *Lecture Notes in Electrical Engineering* 1023: 357–363. Springer, Singapore. https://doi.org/10.1007/978-981-99-0969-8_36
28. Nanyan NF, Ahmad MA, Hekimoğlu B (2024) Optimal PID controller for the DC-DC buck converter using the improved sine cosine algorithm. *Results in Control and Optimization* 14: 100352. https://doi.org/10.1016/j.rico.2023.100352
29. Jabari M, Izci D, Ekinci S, Bajaj M, Zaitsev I (2024) Performance analysis of DC-DC Buck converter with innovative multi-stage PIDn (1+PD) controller using GEO algorithm. *Sci Rep* 14: 25612. https://doi.org/10.1038/s41598-024-77395-6
30. Ersali C, Hekimoglu B, Yilmaz M, Martinez-Morales AA, Akinci TC (2024) Disturbance rejecting PID-FF controller design of a non-ideal buck converter using an innovative snake optimizer with pattern search algorithm. *Heliyon* 10. https://doi.org/10.1016/j.heliyon.2024.e34448
31. Yang X-She (2008) *Nature-Inspired Metaheuristic Algorithms*, Luniver Press, United Kingdom.
32. Yang X-She, He X (2013) Firefly Algorithm: Recent Advances and Applications. *Int J Swarm Intelligence* 1: 36–50. https://doi.org/10.1504/IJSI.2013.055801
33. Fister I, Fister Jr I, Yang XS, Brest J (2013) A comprehensive review of firefly algorithms. *Swarm Evol Comput* 13: 34–46. https://doi.org/10.1016/j.swevo.2013.06.001
34. Wang H, Wang W, Zhou X, Sun H, Zhao J, Yu X, et al. (2017) Firefly Algorithm with Neighborhood Attraction. *Inform Sciences* 382: 374–387. https://doi.org/10.1016/j.ins.2016.12.024
35. Ghasemi M, Mohammadi SK, Zare M, Mirjalili S, Gil M, Hemmati R (2022) A new firefly algorithm with improved global exploration and convergence with application to engineering optimization. *Decision Analytics Journal* 5: 1–18. https://doi.org/10.1016/j.dajour.2022.100125
36. Kalman RE (1960) A new approach to linear filtering and prediction problems. *ASME Journal of Basic Engineering* 82: 35–45. https://doi.org/10.1115/1.3662552
37. Chui CK, Chen G (2009) *Kalman filtering with real time applications*, Berlin Heidelberg: Springer-Verlag, Fourth Edition.
38. Ahmeid M, Armstrong M, Gadoue S, Al-Greer M, Missailidis P (2016) Real-time parameter estimation of DC–DC converters using a self-tuned Kalman filter. *IEEE T Power Electr* 32: 5666–5674. https://doi.org/10.1109/TPEL.2016.2606417
39. Akhlaghi S, Zhou N, Huang Z (2017) Adaptive adjustment of noise covariance in Kalman filter for dynamic state estimation. *IEEE power & energy society general meeting*, 1–5. https://doi.org/10.1109/PESGM.2017.8273755
40. Liu F, Gao Z, Yang C, Ma R (2019) Fractional-order Kalman filters for continuous-time fractional-order systems involving correlated and uncorrelated process and measurement noises. *Trans Ins Meas Control* 41: 1933–1947. https://doi.org/10.1177/0142331218790786
41. Ali M, Mandal S (2022) Kalman filter based control of inverted pendulum system. *IFAC-Papers on Line* 55: 58–63. https://doi.org/10.1016/j.ifacol.2022.04.010

42. Ghosh B, Mandal S (2023) A New Approach for Solar Photovoltaic Parameter Extraction using Metaheuristic Algorithms from Manufacturer Datasheet. *IEEE Open Journal of Instrumentation and Measurement* 2: 1–12. https://doi.org/10.1109/OJIM.2023.3318678

AIMS Press